A Proton Channel Allows a Hydrogen Oxidation Catalyst to Operate at a Moderate Overpotential with Water Acting as a Base

Sheri Lense, Arnab Dutta, John A. S. Roberts, Wendy J. Shaw

Supplementary Information

Summary of shorthand notation:

$[Ni(P^{Cy}_2N^{Bn}_2)_2]^{2+}$	$\mathbf{[1]^{2+}}$
$[Ni(P^{Cy}_2N^{Bn}_2)_2]^{+}$	$\mathbf{[1]^{+}}$
$[Ni(P^{Cy}_2N^{Bn}_2)_2]$	$\mathbf{[1]^{0}}$
$[(H)Ni(P^{Cy}_2N^{Bn}_2)_2]$	$\mathbf{[(H)1]^{+}}$
$[Ni(P^{Cy}_2N^{Bn}_2H)_2]^{2+}$	$\mathbf{[1(H)_2]^{2+}}$
$[Ni(P^{Cy}_2N^{Pyridazine}_2)_2]^{2+}$	$\mathbf{[2]^{2+}}$
$[Ni(P^{Cy}_2N^{Pyridazine}_2)_2]^{+}$	$\mathbf{[2]^{+}}$
$[Ni(P^{Cy}_2N^{Pyridazine}_2)_2]$	$\mathbf{[2]^{0}}$
$[(H)Ni(P^{Cy}_2N^{Pyridazine}_2)_2]$	$\mathbf{[(H)2]^{+}}$
$[Ni(P^{Cy}_2N^{Pyridazine}_2H)_2]^{2+}$	$\mathbf{[2(H)_2]^{2+}}$

General Procedures

Solution state ^{1}H NMR and ^{31}P NMR spectra were recorded on Varian VNMR spectrometers (500 MHz or 300 MHz ^{1}H frequency). All ^{1}H chemical shifts were internally calibrated to the monoprotic solvent impurity and ^{31}P NMR spectra were referenced externally to H_3PO_4 (0 ppm). Elemental analyses were performed by Atlantic Microlab, Norcross, GA, with V_2O_5 as a combustion catalyst.

Synthesis and Materials.

All reactions and manipulations were performed under an N_2 atmosphere using standard Schlenk techniques or a glovebox unless otherwise indicated. Deoxygenated acetonitrile, diethyl ether, THF, ethanol, hexane and dichloromethane were dried using an Innovative Technology, Inc. PureSolv™ solvent purification system. $[Ni(CH_3CN)_6](BF_4)_2$ was prepared as described using literature methods,[1] as was bishydroxymethylcyclohexylphosphine.[2] 3-pyridazinemethanamine was purchased from Synnovator, Inc.

$P^{Cy}_2N^{(3\text{-pyridazyl})methyl}_2$. Bishydroxymethylcyclohexylphosphine (1.61 g, 9.14 mmol) was dissolved in 65 mL ethanol and heated to 70 °C. 3-pyridazinemethanamine (1.00 g, 9.14 mmol) dissolved in 50 mL was then added dropwise over 30 minutes, and the reaction stirred for 20 hours at 70 °C. The reaction was cooled to room temperature, and the solvent removed under vacuum. The resulting solid material was washed with acetonitrile (30 mL x 3) and then dissolved in boiling THF (30 mL) and stored at room temperature for three days. The resulting white precipitate was collected by filtration on a fritted funnel,washed with acetonitrile (5 mL x 2) and dried under vacuum (573.0 mg). The solvent was removed from the filtrate under vacuum, and the resulting residue dissolved in boiling THF (15 mL), and stored at 0 °C for two days. The resulting white precipitate was again collected by filtration on a fritted funnel, washed with acetonitrile (5 mL x 2) and dried under vacuum (198.8 mg). Total yield = 771.8 mg (33.8%). ^{1}H NMR (CD_2Cl_2): δ 9.05 (dd, J = 4.8 Hz, 1.7 Hz, 2H, pyridazine C-*H*), 7.64 (dd, J = 8.4 Hz, 1.7 Hz, 2H, pyridazine C-*H*), 7.45 (dd, J = 4.8 Hz, 8.4 Hz, 2H, pyridazine C-*H*), 4.20 (s, 4H, N-CH_2-pyridazine), 3.12 (s, 8H, P-CH_2-N), 1.66-1.50 (m, cyclohexyl-*H*, 10H), 1.13-1.09 (m, cyclohexyl-*H*, 12H). ^{31}P NMR (CD_2Cl_2): δ -54.2. Anal. Calcd for $C_{26}H_{40}N_6P_2$: C, 62.63; H, 8.09; N, 16.86. Found: C, 62.58; H, 8.19; N, 16.66.

[Ni(P$^{Cy}_2$N$^{(3\text{-pyridazyl)methyl}}_2$)$_2$](BF$_4$)$_2$ ([2]$^{2+}$). [Ni(CH$_3$CN)$_6$](BF$_4$)$_2$ (57.0 mg, 0.12 mmol) in 3 mL acetonitrile was added to P$^{Cy}_2$N$^{(3\text{-pyridazyl)methyl}}_2$ (132.6 mg, 0.27 mmol). The deep purple reaction was stirred for two hours, and then filtered. The solvent was removed under vacuum and the dark purple residue dried under vacuum for four hours. Total yield = 105.0 mg (71%). ^{31}P NMR (CD$_3$CN): δ 6.2. ^{1}H NMR (CD$_3$CN): δ 9.21 (dd, J = 4.6 Hz, 1.8 Hz, 4H, pyridazine C-*H*), 7.67 (m, 8H, pyridazine C-*H*), 4.07 (s, 8H, N-C*H*$_2$-pyridazine), 3.35 (d, J = 13.7 Hz, 4H, P-C*H*$_2$-N), 3.20 (m, 8H, P-C*H*$_2$-N), 2.95 (d, J = 12.8 Hz, 4H, P-C*H*$_2$-N), 1.96-1.14 (m, 44H, cyclohexyl-*H*). Anal. Calcd for C$_{52}$H$_{80}$B$_2$F$_8$N$_{12}$NiP$_4$: C, 50.80; H, 6.56; N, 13.67. Found: C, 50.02; H, 6.83; N, 13.22. ESI MS (MeCN): m/z [M]$^+$: expt. 1225.56 (calcd. 1225.68).

[Ni(I)(P$^{Cy}_2$N$^{(3\text{-pyridazyl)methyl}}_2$)$_2$](BF$_4$) ([2]$^+$). [Ni(I)(P$^{Cy}_2N^{(3\text{-pyridazyl)methyl}}_2$)$_2$](BF$_4$) was prepared *in situ* for electrochemistry experiments. (9.2 mg; 7.5 mmol) and CoCp*$_2$ (2.5 mg; 7.5 mmol) were combined in 10 mL MeCN (0.2 M ^{n}Bu$_4$N$^+$PF$_6^-$) and stirred for 30 min, during which time the solution color changed from purple to yellow. The solution was filtered through glass wool and celite to remove any Ni(0) byproduct. Anodic voltammetry beginning at -0.96 V vs. FeCp$_2^{+/0}$ revealed no initial reduction or oxidation current, indicating that the bulk solution contained neither Ni(II) nor Ni(0) in appreciable quantities.

[Ni(P$^{Cy}_2$N$^{(3\text{-pyridazyl)methyl}}_2$)$_2$] ([2]^0). P$^{Cy}_2N^{(3\text{-pyridazyl)methyl}}_2$ (17.5 mg, 35 mmoles) and [Ni(MeCN)$_6$](BF$_4$)$_2$ (8.4 mg, 18 mmoles) were placed in 1 mL of MeCN and stirred for one hour. Tetramethylguanidine (4.2 mg, 37 mmoles) in 1 mL MeCN was added. Hydrogen was bubbled through the solution for five minutes, and the reaction was allowed to sit for four days, during which time **[2]^0** precipitated as a yellow solid. The product was washed with additional acetonitrile (~ 20 mL) and dried under vacuum. Yield: 9.1 mg, 48%. Re-crystallization by slow diffusion of ether into a dichloromethane solution of the product on a smaller scale yielded X-ray quality orange, block shaped crystals. ^{31}P{^{1}H} NMR (CD$_2$Cl$_2$): δ (ppm) 9.8. ^{1}H NMR. (CD$_2$Cl$_2$): δ 9.12 (d, J = 4.7 Hz, 4H, pyridazine C-*H*), 7.47 (dd, 8.3, 5.0 Hz, 4H, pyridazine C-*H*), 7.43 (d, 8 Hz, 4H, pyridazine C-*H*), 4.03 (s, 8H, N-C*H*$_2$-pyridazine), 2.61 (br, 16H, P-C*H*$_2$-N), 1.96-1.14 (m, 44H, cyclohexyl-*H*). ESI MS (MeCN): m/z [M+H]$^+$: expt. 1053.51 (calcd. 1053.62).

Attempted Preparation of [Ni(P$^{Cy}_2$N$^{Pyridine}_2$)$_2$]. We were unable to prepare the P$^{Cy}_2$N$^{Pyridine}_2$ in reasonable purity. Often for these complexes, the metal complex can still be prepared in high purity by preparing the Ni(II) species with the crude ligand, adding H$_2$ and deprotonating this species to isolate the Ni(0) species (similar to the description above for the preparation of **[2]^0**), which has very different solubility properties than the ligand or Ni(II) species. In the case of [Ni(P$^{Cy}_2$N$^{Pyridine}_2$)$_2$]$^{2+}$, the addition of hydrogen did not result in changes in the ^{1}H or ^{31}P NMR spectra, indicating that H$_2$ did not add. This is likely due to the stronger σ-donating properties of the pyridine ligand, causing it to associate to the metal. Unfortunately, due to the impurity of the complex, we were unable to unambiguously confirm this hypothesis.

p*K*$_a$ Measurements.

The p*K*$_a$ of [Ni(P$^{Cy}_2$N$^{(3\text{-pyridazyl)methyl}}_2$H)$_2$](BF$_4$)$_2$ ([**2(H)$_2$**]$^{2+}$) was measured as described for similar complexes [Ni(P$^{Cy}_2$N$^{R'}_2$H)$_2$](BF$_4$)$_2$[3] with the following adjustments: **[2]$^{2+}$** (5.7 mg, 0.0046 mmol) was dissolved in 0.6 mL CD$_3$CN, transferred to an NMR tube and the solution sparged with H$_2$ to form [**2(H)$_2$**]$^{2+}$. The solution was then titrated with a solution of *p*-anisidine in CD$_3$CN (0.199 M). The ^{1}H and ^{31}P NMR spectra were recorded at -45 ºC, since the hydride formed from deprotonation of [**2(H)$_2$**]$^{2+}$ exchanges with the **e/x** isomer of [**2(H)$_2$**]$^{2+}$ and is difficult to quantify at room temperature.

Estimation of the p*K*$_a$ of the endo-endo species. Due to the small population of the **e/e** or **e/x** isomers, the p*K*$_a$ of the endo protonated amine could not be directly determined. However, the p*K*$_a$ of the endo-endo species can be estimated using established thermodynamic relationships[4] and the following equation[5]:

$$\Delta G^{o}_{H2} = 76 - (\Delta G^{o}_{H-} + 1.364 * pK_a(NH)) \quad (1)$$

where:

ΔG^{o}_{H2}=the free energy of hydrogen addition to the complex
ΔG^{o}_{H-}=the hydride donor ability
$pK_a(NH)$=the pKa of the pendant amine
76 kcal/mol is the heterolytic cleavage of H_2 ($H_2 \rightarrow H^+ + H^-$)

The ΔG^{o}_{H2} determines whether or not adding hydrogen is favorable. We know from experimental observations that values of 2.7 kcal/mol uphill require H_2 pressure of 1000 psi to add H_2.[6] Conversely, a value of 3.1 kcal/mol downhill results in the quantitative addition of H_2 at 1 atm.[7]

From this knowledge, two different scenarios can be considered. The first is that these established relationships hold and the following analysis can be performed. From the established thermodynamic relationships[4] (y=20.817x + 76.765, where x is the Ni(II/I) couple in MeCN and y= ΔG^{o}_{H-}), we can estimate the ΔG^{o}_{H-} based on the Ni(II/I) couple to be 60.5 kcal/mol (nearly identical to that of the control complex, $[Ni(P^{Cy}_2N^{Bn}_2)_2]^{2+}$, due to the very similar Ni(II/I) couples). If ΔG^{o}_{H2} is assumed to be 2 kcal/mol downhill, a reasonable assumption since the addition of H_2 is essentially quantitative, the pK_a(NH) is estimated to be 12.8. If a more conservative estimate of ΔG^{o}_{H2}=-1 kcal/mol is used, the pK_a(NH)=12.0. Similar complexes with pK_a values of 12.5 have been reported and have rates of 3-5 s^{-1} using triethyl amine, similar to the rate observed here with triethyl amine (3 s^{-1}), suggesting that these pK_a(NH) values are not unreasonable.[3]

A second possibility is that the pK_a of the pendant amine drops more than that estimated based on the thermodynamic relationships, but is deprotonated due to the pyridazine so quickly that the estimates are skewed. Because we know deprotonation happens very quickly (CV's give us a lower estimate of 0.2 to 1 s^{-1}), this mechanism cannot be ruled out. We are currently performing computational studies to assess the pK_a value of the endo-endo species to provide a more clear role of the mechanism of deprotonation.

Electrochemical Studies

Cyclic Voltammetry. The acetonitrile used for electrochemical measurements was purchased from Burdick & Jackson. The triethylamine used for electrochemical measurements was distilled over CaH_2 and then degassed using the freeze−pump−thaw method, and the water (18 MΩ) used for electrochemical measurements was sparged with N_2 before use. Catalyst concentration was 0.75 mM in all cases unless otherwise noted, beginning with the Ni^{I} or Ni^{II} species as noted. Cyclic voltammetry experiments were carried out on a computer-aided CH Instruments 1100 A potentiostat in a glovebox with an N_2 atmosphere in 0.2 M $^{n}Bu_4N^{+}PF_6^{-}$/acetonitrile at a scan rate of 50 mV/s unless otherwise noted. The working electrode used was a glassy-carbon disk, and the counter electrode was a glassy-carbon rod. A silver wire was used as a pseudo reference electrode. Decamethylcobaltocenium hexafluorophosphate ($CoCp^*_2{}^{+}PF_6^{-}$, −1.94 V vs $FeCp_2^{+/0}$ in acetonitrile) or cobaltocenium hexafluorophosphate ($CoCp_2^{+}PF_6^{-}$, −1.33 vs $FeCp_2^{+/0}$ in acetonitrile) were used as internal standards to reference the potentials of the Ni(II/I) and Ni(I/0) redox couples to the ferrocenium/ferrocene couple. Three trials were run for each type of base (water and triethylamine). At least one trial in each set was run with either $CoCp_2^{+}$ or $CoCp^*_2{}^{+}$ as an internal reference, and at least one trial in each set was run without addition of an internal reference in order to ensure that the internal reference did not influence the rates measured.

Low Temperature NMR Studies.

The sample was placed in a J Young tube fitted with PEEK tubing, placed in the NMR magnet and cooled to -65 °C. H_2 was introduced through PEEK tubing via an ISCO pump. Spectra were taken

at room temperature and at -65 °C before H_2 (ultra-high purity) was added. NMR acquisition began immediately following the addition of H_2 and was monitored for ~ 2 hours. Each sample was run at least three times for reproducibility.

Mass spectrometry.

MS analysis was performed using a LTQ Orbitrap Velos mass spectrometer (Thermo Scientific, San Jose, CA) outfitted with a custom electrospray ionization (ESI) interface. Electrospray emitters were custom made using 360 μm o.d. × 20 μm i.d. chemically etched fused silica.[8] The ion transfer tube temperature and spray voltage were 300 ºC and 2.2 kV, respectively. Orbitrap spectra (AGC 1x106) were collected from 600-2000 m/z at a resolution of 100k or 300-600 m/z at a resolution of 100k. Samples were directly infused using a 250 μL Hamilton syringe at a flow rate of 1 μL/min.

Supplementary Figures and Tables

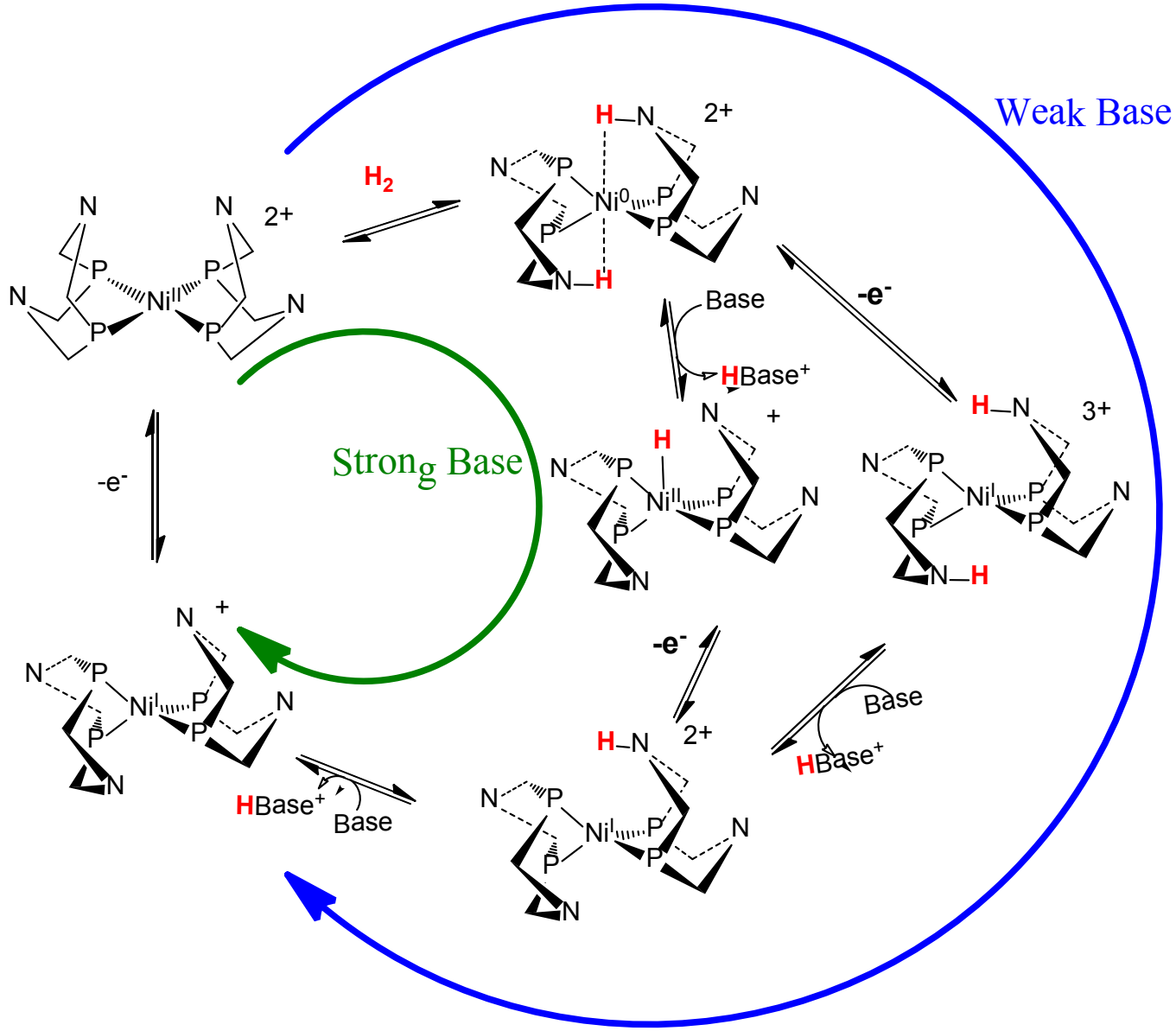

Figure S1. The catalytic cycle proceeds through a different mechanism depending on the strength of the base used, as previously reported.[3, 9] For strong bases such as triethylamine, the cycle highlighted with the green arrow is observed, where deprotonation to the Ni(II) hydride is followed by oxidation. When weak bases such as water are used, the outer mechanism, highlighted with the blue arrow, is observed, where oxidation occurs first, followed by deprotonation.

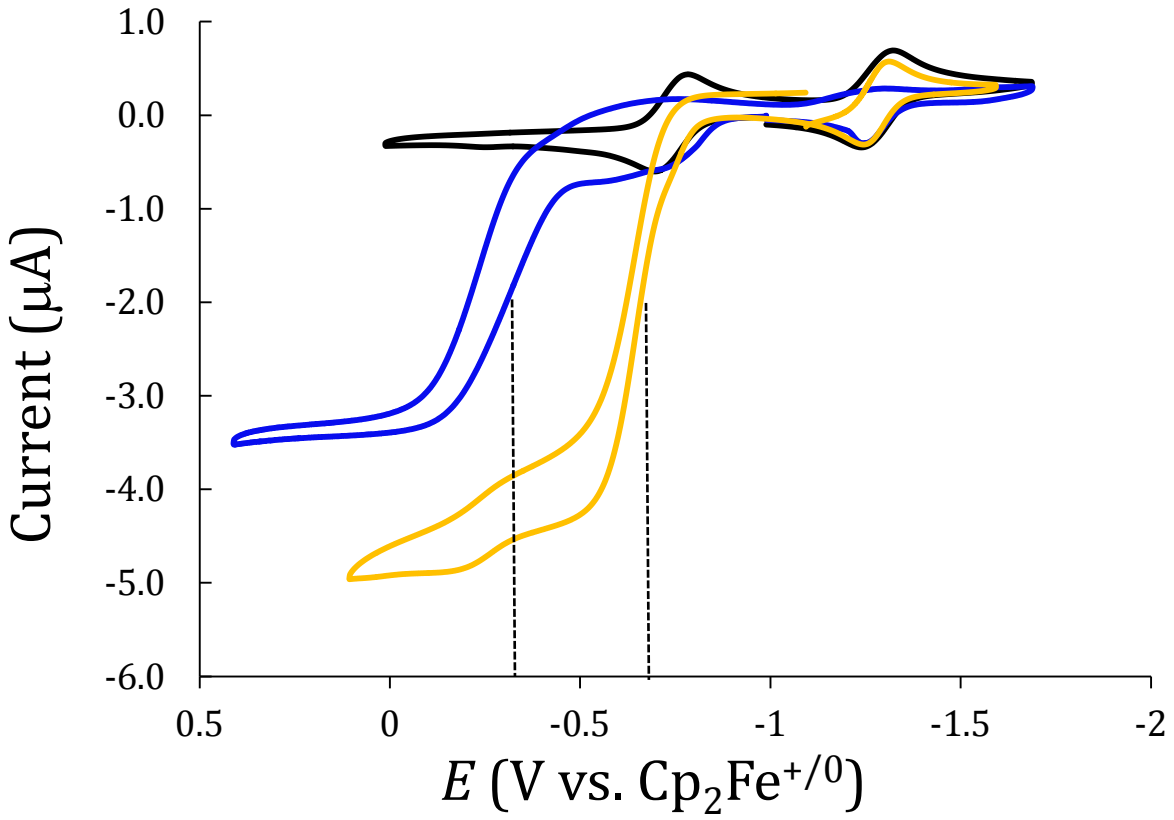

Figure S2. Cyclic voltammograms of a 0.75 mM solution of $\mathbf{[1]^+}$ at a scan rate of 50 mVs^{-1} under N_2 (black), under H_2 in the presence of 5.0 M H_2O (blue) and under H_2 in the presence of 0.03 M triethylamine (orange). In the presence of water, the catalytic wave occurs at the endo-exo $\mathbf{[1(H)_2]^{+/0}}$ couple (~-0.3 V) and in the presence of triethylamine the catalytic wave occurs at the Ni(II) hydride couple (~-0.7 V). The difference in mechanism results in a much higher overpotential, where $E_{cat/2}$ is indicated for each process with dashed lines. Conditions: 0.2 M $^nBu_4N^+PF_6^-$ acetonitrile solutions, glassy-carbon working electrode.

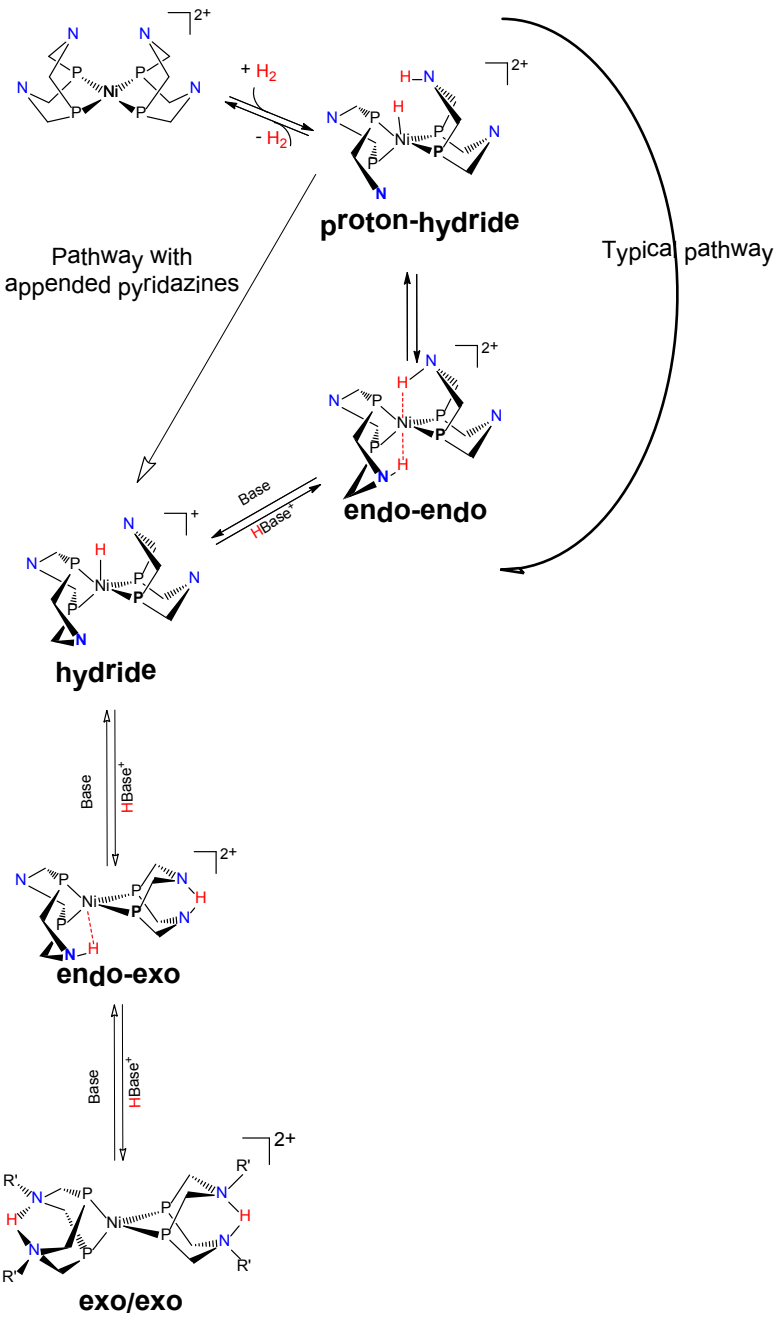

Figure S3. The initial product of H_2 addition for $[Ni(P^R{}_2N^{R'}{}_2)_2]$ complexes has been suggested by computational methods to be the proton hydride.[10] For $[Ni(P^{Cy}{}_2N^{Bn}{}_2H)_2]^{2+}$ (**$[1(H)_2]^{2+}$**), this quickly transforms to the endo-endo species, the first experimentally observed species. Isomerization occurs by deprotonation of the endo-endo species to result in the hydride (once one pendant amine is deprotonated, the remaining proton moves to the Ni). Reprotonation in the exo position yields the endo-exo isomer (upon reprotonation in the exo position, the hydride moves out to the endo positioned amine). Deprotonation of the second endo positioned amine and reprotonation in the exo position results in the exo-exo isomer. Details can be found in O'Hagan, *et al.*[11] For **$[2(H)_2]^{2+}$**, the endo-endo species is not observed, suggesting that this species is either a high energy intermediate or is not formed, bypassing the stabilized endo-endo species, as shown.

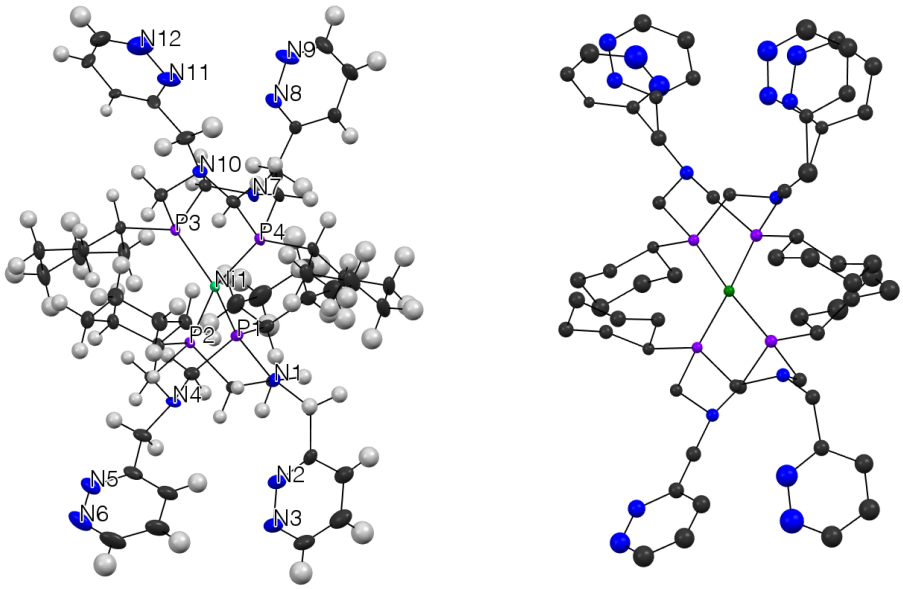

Figure S4. Crystal structure of [Ni($P^{Cy}_2N^{(3\text{-pyridazyl)methyl}}_2$)$_2$] (**[2]^0**) showing hydrogen atoms (left) and disorder (right). X-ray quality crystals of **[2]^0** were grown by sparging an acetonitrile solution of [Ni($P^{Cy}_2N^{(3\text{-pyridazyl)methyl}}_2$)$_2$]($BF_4$)$_2$ (**[2]$^{2+}$**) with H_2 followed by addition of two equivalents of tetramethylguanidine. The reaction was allowed to sit for several days, over which time **[2]^0** precipated as orange block-shaped crystals. The crystals were mounted on a MiTeGen MicroMounts pin using Paratone-N oil and cooled to 140 K. Data were collected on a Bruker-AXS CCD diffractometer with 0.71073 Å Mo K∝ radiation. The crystal was a non-merohedral twin. Cell parameters were retrieved using Bruker APEX II software[12] and the raw data was integrated using SAINTPlus.[13] The cells and orientation matrices were found using Cell_Now.[14] A multi-component integration was performed using SAINTPlus,[13] and the data was processed using TWINABS.[15] The structures were solved using direct methods and refined by a least-squares method on F^2 using the SHELXTL program package.[12] Space groups were chosen by analysis of systematic absences and intensity statistics. The final refinement included the twin fractions (BASF) and used the HKLF 5 format file.

Complex	[$Ni^0(P^{Cy}_2N^{Pyridazine}_2)_2$]	[$Ni^0(P^{Cy}_2N^{Bn}_2)_2$]
Ni-P(1, 2, 3, 4) (Å)	2.1290(9), 2.1283(8), 2.1279(8), 2.128(1)	2.1376(3), 2.1375(3), 2.1302(3), 2.1301(3)
P1-Ni-P2, P3-Ni-P4 (deg)	85.62(3), 85.68(3)	85.450(9), 85.446(9)
Dihedral angle (deg)	89.54	88.67
R1	0.0582	0.0364
Space group	*P*-1	*C*2/*c*
N1-N2, N4-N5, N7-N8, N10-N11 (Å)	3.082, 3.549, 2.850, 2.984	N/A
N5-N1, N2-N4, N7-N11, N10-N8 (Å)	6.310(5), 4.566(5), 4.866(7), 4.518(8)	N/A

Table S1. Structural parameters of **[2]^0**. **[1]^0** is shown for comparison,[3] and demonstrates the structural similarity of the two complexes.

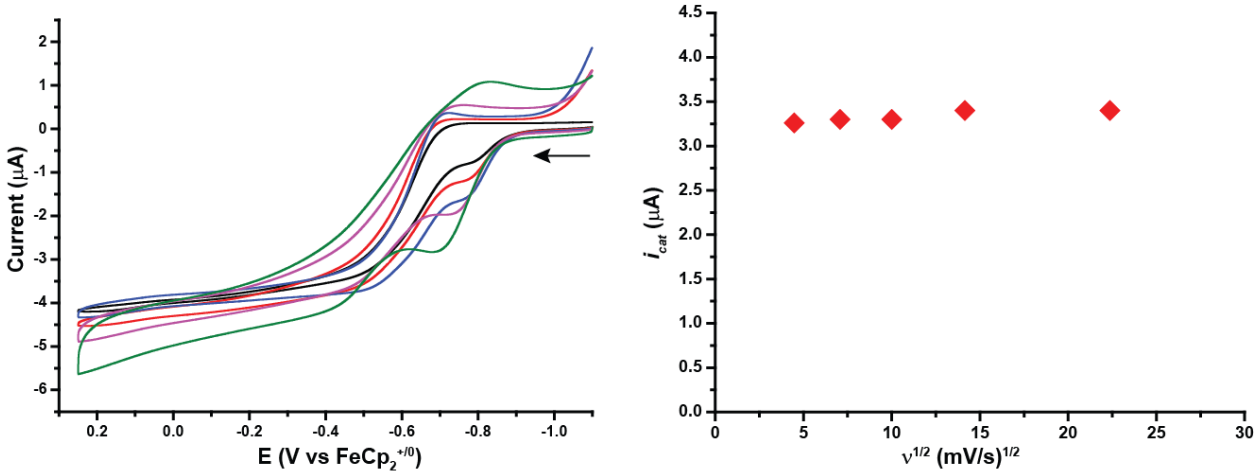

Figure S5. Scan rate (υ) independence observed for the H_2 oxidation wave when water (5 M) and H_2 are added to **[2]**$^{2+}$. Left, CV's used to obtain the plot of i_c vs. $\upsilon^{1/2}$ shown on the right. Scan rates are: 20 (black), 50 (red), 100 (blue), 200 (magenta) and 500 (green) mV/s. Catalyst concentration: 0.75 mM. Conditions: 0.2 M $^{n}Bu_4^{+}PF_6^{-}$ acetonitrile solutions, glassy-carbon working electrode.

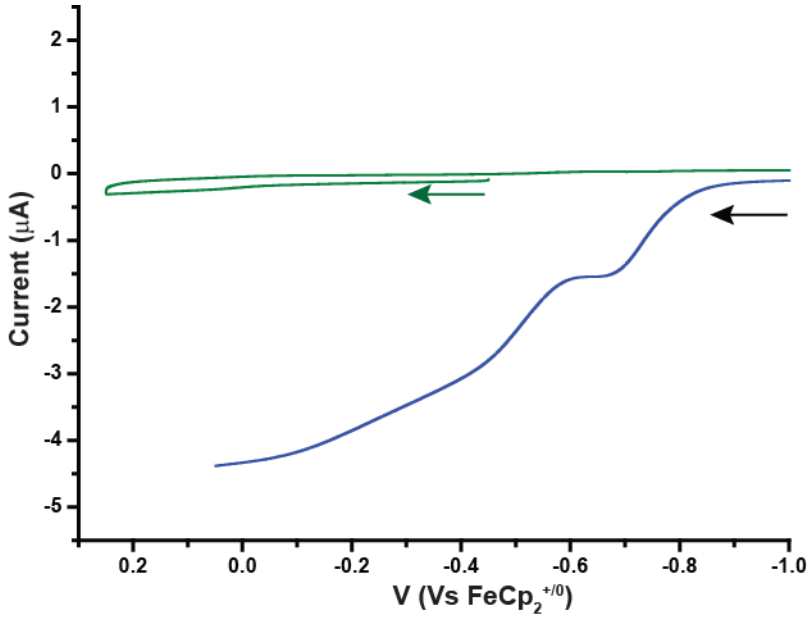

Figure S6. Hydrogen oxidation is demonstrated to utilize a homogeneous catalyst based on the electrochemistry rinse test. This test was executed as the following series of experiments. A cyclic voltammogram was recorded with a freshly polished glassy carbon working electrode for $\mathbf{[2]}^{2+}$ (0.75 mM) in acetonitrile with 5.0 M water (0.1 M $^{n}Bu_4N^{+}PF_6^{-}$) under one atm of H_2 (blue line) up to 0.05 V (vs $FeCp_2^{+/0}$). A subsequent voltammogram was recorded (starting from -0.45 V) with the same electrode from the previous experiment after rinsing (but no polishing) and transferring to a fresh solution of acetonitrile (containing 5.0 M water with 0.1 M $^{n}Bu_4N^{+}PF_6^{-}$) with no Ni catalyst. No significant residual current enhancement was detected during the last scan in the H_2 oxidation direction confirming the homogeneous nature of the catalyst during H_2 oxidation.

Bulk Electrolysis. Bulk electrolysis measurements were performed on 4.0 mL of a 1.0 mM solution of **[2]**$^{2+}$ in acetonitrile containing 5.0 M H_2O, 0.2 M $^nBu_4N^+PF_6^-$ and 1 mM $CoCp_2^+PF_6^-$ as a reference. In order to determine the accurate potential, before performing the bulk electrolysis measurement, cyclic voltammetry experiments were performed both under N_2 and after sparging the solution with H_2, on a computer-aided BASI EC Epsilon potentiostat. The working electrode used was a glassy-carbon disk, and the counter electrode was a platinum coiled wire in a glass compartment containing 0.2 M $^nBu_4N^+PF_6^-$ acetonitrile and a Vycor tip. A Ag^+/AgCl reference electrode was used.

Bulk electrolysis measurements were then performed on a computer-aided BASI EC Epsilon potentiostat in conjunction with a BASI PWR-3 Power Module in order to boost the compliance voltage. The working electrode was a carbon mesh cylinder into which a copper wire had been threaded, the counter electrode was a platinum coiled wire in a glass compartment containing a 0.2 M $^nBu_4N^+PF_6^-$acetonitrile solution and a Vycor tip. A Ag^+/AgCl reference electrode was used. The bulk electrolysis measurement was run at -0.65 V vs. $Cp_2Fe^{+/0}$. The solution was continuously sparged with hydrogen and stirred vigorously during the measurement. After one hour and forty-five minutes, 9.5 C of charge were passed, which corresponded to 22.7 equivalents of electrons/catalyst. A cyclic voltammetry measurement of the solution was repeated after the measurement, confirming that the potential had not shifted during the course of the bulk electrolysis measurement.

The amount of H_3O^+ produced was quantified using ^{1}H NMR. The chemical shifts of the aromatic protons in *p*-anidisine vary depending on the acidity of the solution. A calibration curve was created by adding acid $[(Et_2O)_2H]^+B(C_6F_5)_4^-$ to a 100.0 mM solution of *p*-anisidine in 0.2 M nBu_4PF_6, acetonitrile/5.0 M H_2O, and measuring the resulting change in ^{1}H chemical shifts upon protonation of *p*-anisidine (Figure S7). 100.0 mM *p*-anisidine was added to aliquots of the bulk electrolysis solution that had and had not undergone bulk electrolysis. In the solution that had not undergone bulk electrolysis, the ^{1}H chemical shifts of *p*-anisidine were the same as those of *p*-anisidine in the absence of acid, whereas in the solution that had undergone bulk electrolysis, the ^{1}H chemical shifts of *p*-anisidine corresponded to the addition of 20.5 equivalents acid/catalyst, 90% of H_3O^+ based on the charge passed. The ^{31}P NMR spectrum confirmed that no decomposition of the catalyst had occurred during the experiment based on the presence of the resonance for **[2]**$^{2+}$ and the absence of any new resonances.

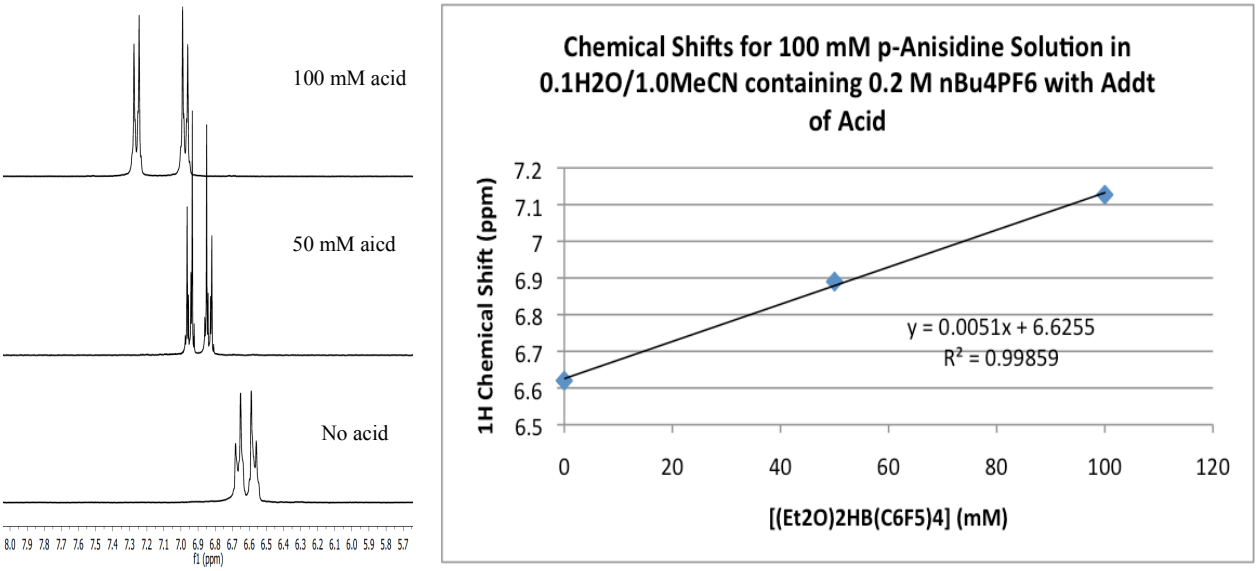

Figure S7. NMR spectra (left) used to creat the calibration curve (right) to quantify the amount of acid generated during the bulk electrolysis expreriment using **[2]**$^{2+}$ in 5M water. This curve was generated by adding acid $[(Et_2O)_2H]^+B(C_6F_5)_4^-$ to a 100.0 mM solution of *p*-anisidine in 0.2 M nBu_4PF_6, acetonitrile/5.0 M H_2O.

Open Circuit Potential (OCP) Measurements. The OCP experiment measures an equilibrium potential governed by the redox reactions occurring at the working electrode according to the Nernst equation. When the only redox process is reaction 1, the open circuit potential will be E_{BH+} and will depend on the activities of the acid, base, and hydrogen.

(1) $$BH^+_{(soln)} + e^- \overset{E_{BH^+}}{\rightleftharpoons} B_{(soln)} + \tfrac{1}{2} H_{2(g)}$$

Measurement of E_{BH+} of H_2O-MeCN solutions of varying acidity. Due to the small autodissociation constant for water, acid and base activities will be exceedingly low, resulting in potentially large errors in the measurement. We therefore determined OCP values for two solutions buffered using Et_3NH^+:Et_3N, one having an acid:base ratio chosen to give a more positive OCP value than the unbuffered case, and the other giving a more negative value. Serial dilution of these two buffered solutions gave OCP values approaching the value measured for the unbuffered solution (Figure S10). A stock electrolyte solution, MeCN (0.50 M H_2O, 0.1 M $^n Bu_4N^+PF_6^-$), was prepared by diluting H_2O (2.253 g, 125.1 mmol) and $^n Bu_4N^+PF_6^-$ (969.3 mg) to 25.0 mL using MeCN (Burdick and Jackson). Stock solutions of acid (0.10 M $[(Et_2O)_2H]^+B(C_6F_5)_4^-$) or base (0.10 M Et_3N) were prepared by diluting $[(Et_2O)_2H]^+B(C_6F_5)_4^-$ (415.0 mg, 0.501 mmol) or Et_3N (50.5 mg, 0.499 mmol) to 5.0 mL using the electrolyte solution. Buffer solutions with $(Et_2O)_2H^+$:Et_3N = 1:2 and 1:100 were prepared by adding 0.500 mL and 0.010 mL of acid stock solution to 1.00 mL portions of base stock solution. The following sequence of measurements was executed for each buffer solution: a crystal of decamethylferrocene (Fc*) was added and the solution was sparged 5 min using H_2 bubbled through vigorously stirred MeCN (5M H_2O). Paired OCP-CV measurements were made as described in ref.[16] A 0.20 mL aliquot of the solution was then diluted by adding it to 0.80 mL of stock electrolyte solution. This solution was sparged with H_2, and paired OCP-CV measurements were again made. This sequence of serial dilution and measurement was repeated six times. The first system, having acid:base = 1:2 (intial [acid] = 33 mM, [base] = 67 mM) showed a negative shift in OCP with increasing dilution, and the second, having acid:base = 1:100 (intial [acid] = 1.0 mM, [base] = 99 mM) showed a positive shift. Large changes in OCP at dilution factors smaller than 10^{-3} were observed for both and were consequently discarded. Data appear in Figure S8.

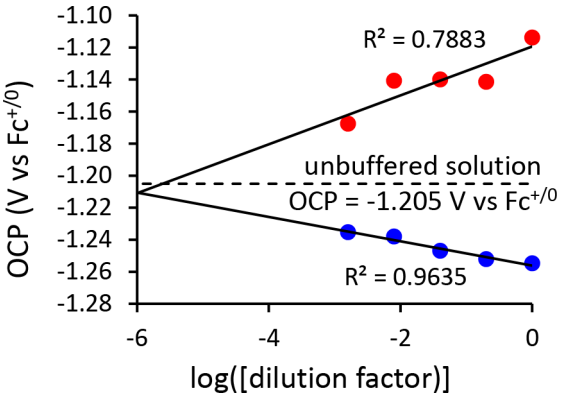

Figure S8. Open circuit potential vs. log(dilution factor) for serially diluted buffered solutions. Acid:base = 1:2 (red); acid:base = 1:100 (blue); unbuffered solution (single-point measurement; dashed line). The OCP for the unbuffered solution is -1.205 V vs. $Fc^{+/0}$.

Electrochemistry analysis under H_2. In these experiments, the complexes are introduced as the Ni(I) species, where a positive potential sweep results in a Ni(I/II) oxidation, triggering H_2 addition and allowing the observation of the kinetic H_2 addition products. The voltammograms of these two complexes under H_2 are significantly different (Fig. S9). For $[\mathbf{1}]^+$, H_2 addition following $Ni^{I/II}$ oxidation results in the observation of unique redox couples for each isomer ($E_{p/2}$, or the potential at ½ the maximum peak current): **e/e** (0.0 V), the **e/x** (−0.30 V) and the **x/x** (−0.67 V) (blue trace), similar to other complexes of this type.[3, 17] In contrast, for $[\mathbf{2}]^+$, H_2 addition following the $Ni^{I/II}$ oxidation affords a complex wave, with E_p = −0.43 V, which we assign to the **e/x** isomer, based on the following: the possible contributions to this wave include the **e/e**, **e/x**, **x/x** and the Ni(II) hydride. This wave is significantly less positive (500 mV) than the typically observed **e/e** isomer (Fig. S9).[3] Studies starting with the **x/x** isomer, generated by equilibrating a solution of $[\mathbf{2}]^{2+}$ with H_2 (Fig. S10), show that this isomer oxidizes at −0.68 V; this feature is not observed in the non-equilibrated solution.[18] Therefore, the electrochemistry data, along with NMR spectra of similar solutions (same solvent but higher concentration) at room temperature, are most consistent with the assignment of this wave (Fig. S9) as the oxidation of the **e/x** isomer, but we cannot definitively rule out a contribution from the hydride. Regardless of the identity of the species, the observation of the **e/x** isomer or the hydride provides a lower limit for the rate constant for deprotonation and/or isomerization of 0.2-1 s^{-1}.

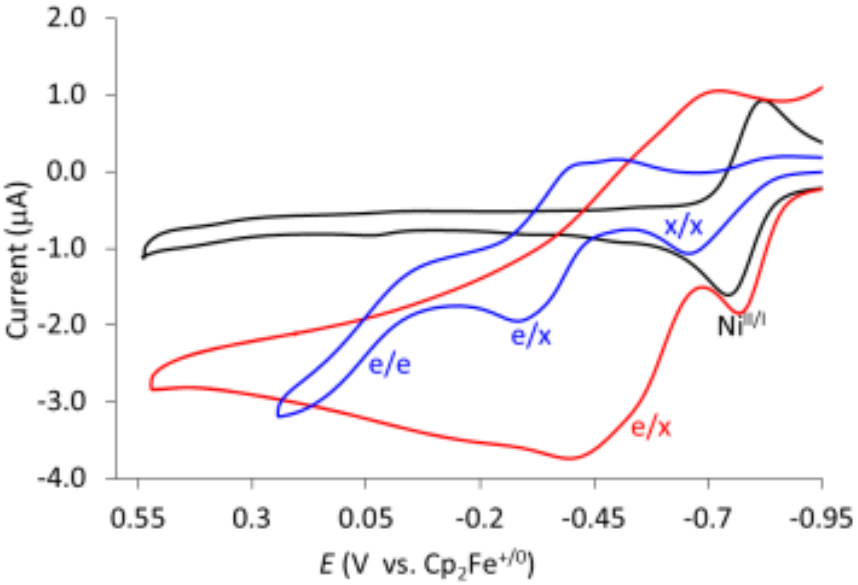

Fig. S9 Left: Cyclic voltammograms (CV's) of 0.75 mM $[\mathbf{2}]^+$ under N_2 (black) and H_2 (red) and 0.75 mM $[\mathbf{1}]^+$ under H_2 (blue). Conditions: 0.2 M $^nBu_4^+PF_6^-$ acetonitrile solutions, 100 mV/s, glassy-carbon working electrode.

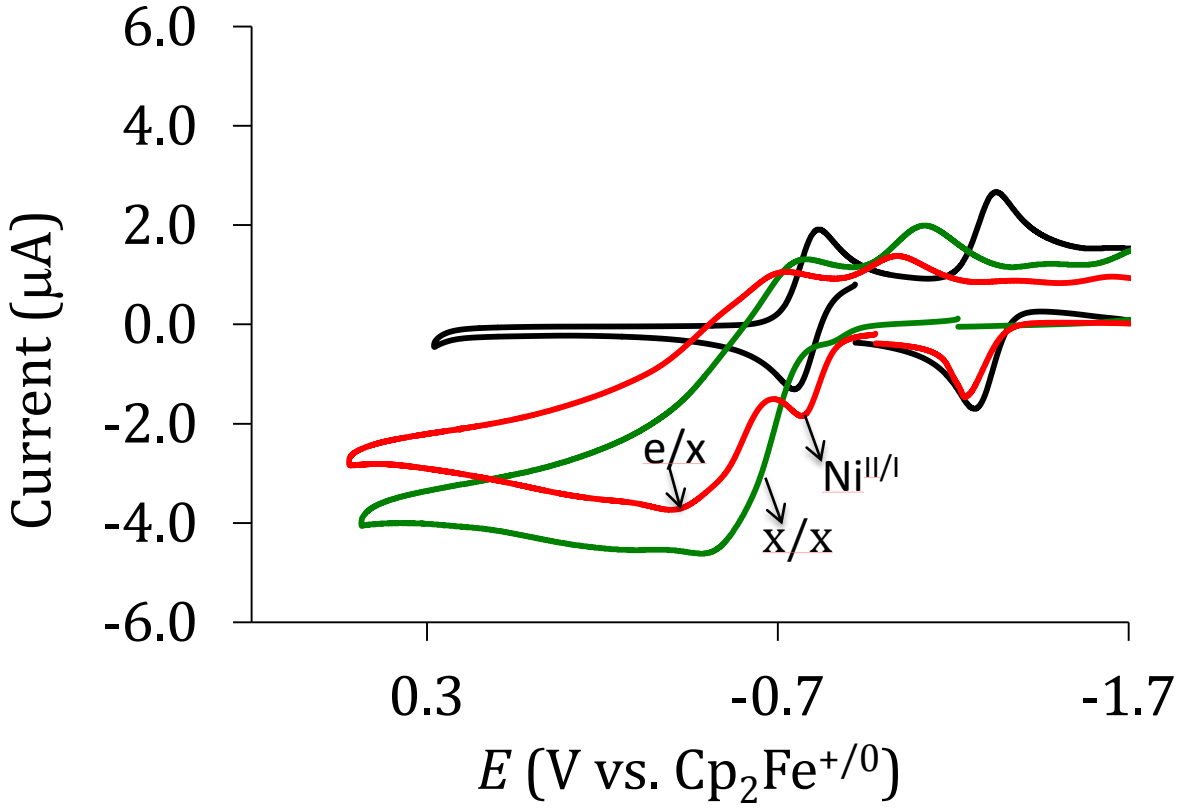

Figure S10. Electrochemistry of 0.75 mM $[\mathbf{2}]^{+}$ under N_2 (black) and H_2 (red) and $[\mathbf{2}]^{2+}$ after one hour under H_2 (green). The $[\mathbf{2}]^{2+}$ solution was followed by ^{31}P NMR spectroscopy, which indicated that it had reached an equilibrium distribution of 95% **x/x** isomer before the voltammogram was recorded. $[\mathbf{2}]^{+}$ does not react with H_2 until oxidation from Ni^{I} to Ni^{II} occurs, allowing kinetic and equilibrium products to be identified and distinguished. Conditions: 0.2 M $^{n}Bu_4^{+}PF_6^{-}$ acetonitrile solutions, 100 mV/s, glassy-carbon working electrode.

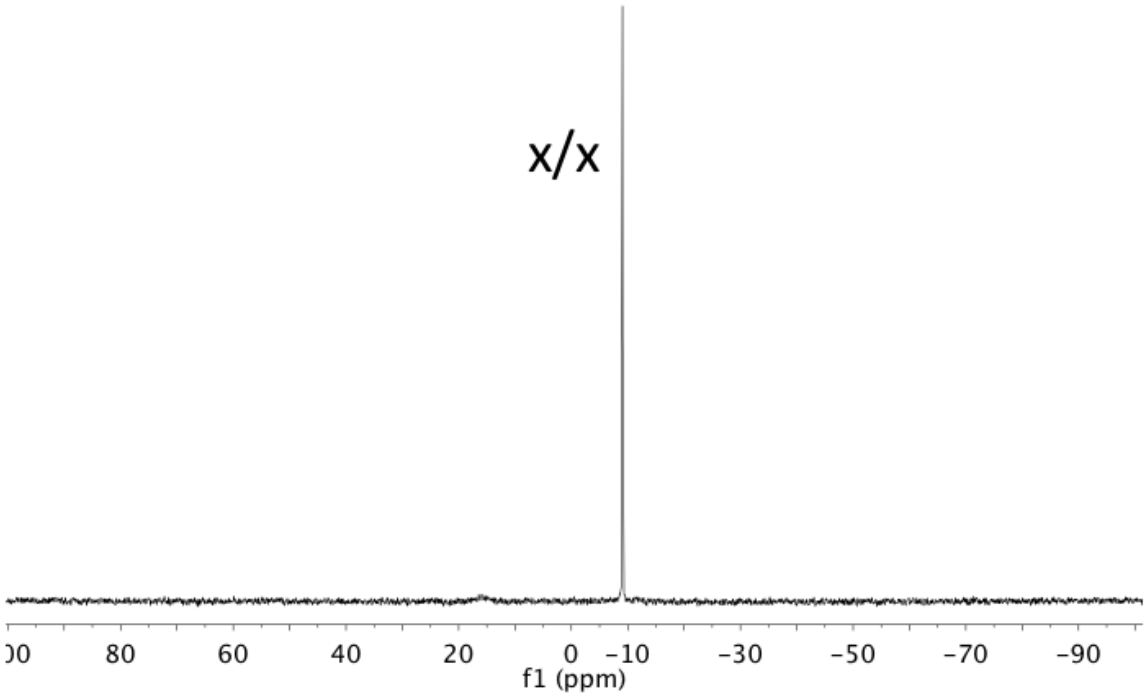

Figure S11. ^{31}P NMR spectrum of $\mathbf{[2(H)_2]^{2+}}$ (9.1 mM) immediately following addition of H_2 at room temperature showing the predominance of the **x/x** species. In contrast, $\mathbf{[1(H)_2]^{2+}}$ is predominantly **e/e** at a similar time and takes several days to convert to **x/x**.[11]

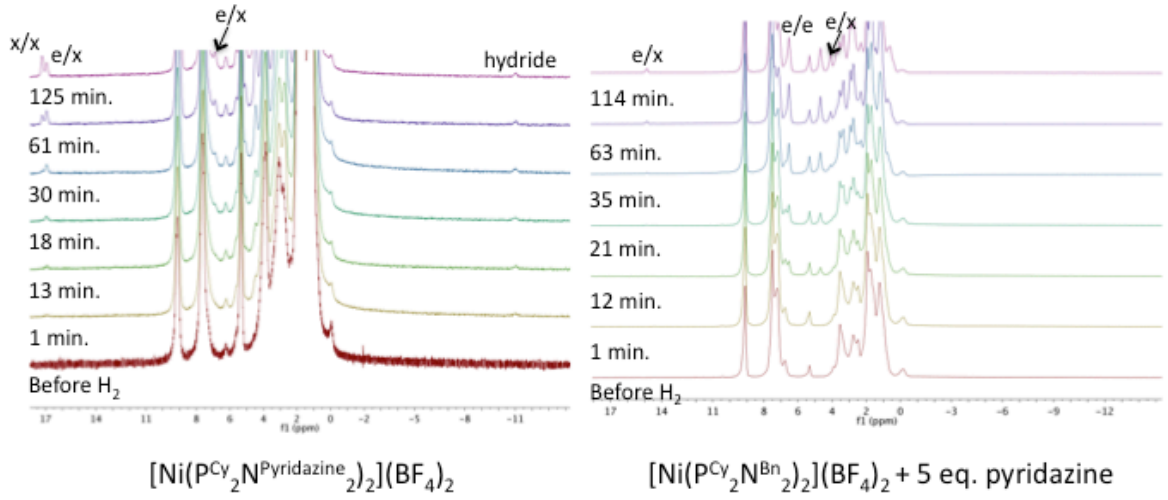

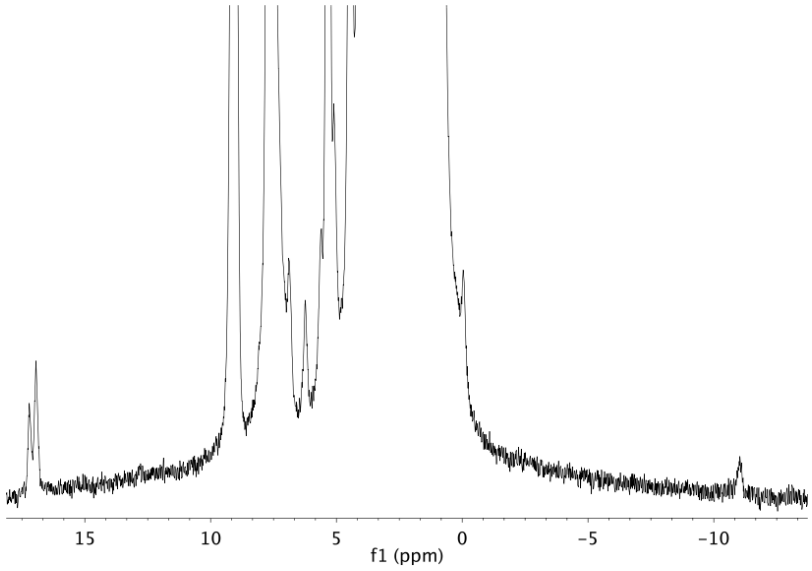

Figure S12. Top: ^{1}H NMR corresponding to the ^{31}P NMR in Figure 4, supporting the formation of hydride and the **e/x** for **[2]**$^{2+}$ + H_2. Note that no hydride and very little **e/x** are observed in the $[Ni(P^{Cy}{}_2N^{Bn}{}_2)_2]^{2+}$ (**[1]**$^{2+}$) + H_2 with externally added pyridazine. Bottom: The spectrum collected at 125 min for **[2]**$^{2+}$ + H_2 is magnified to show the hydride.

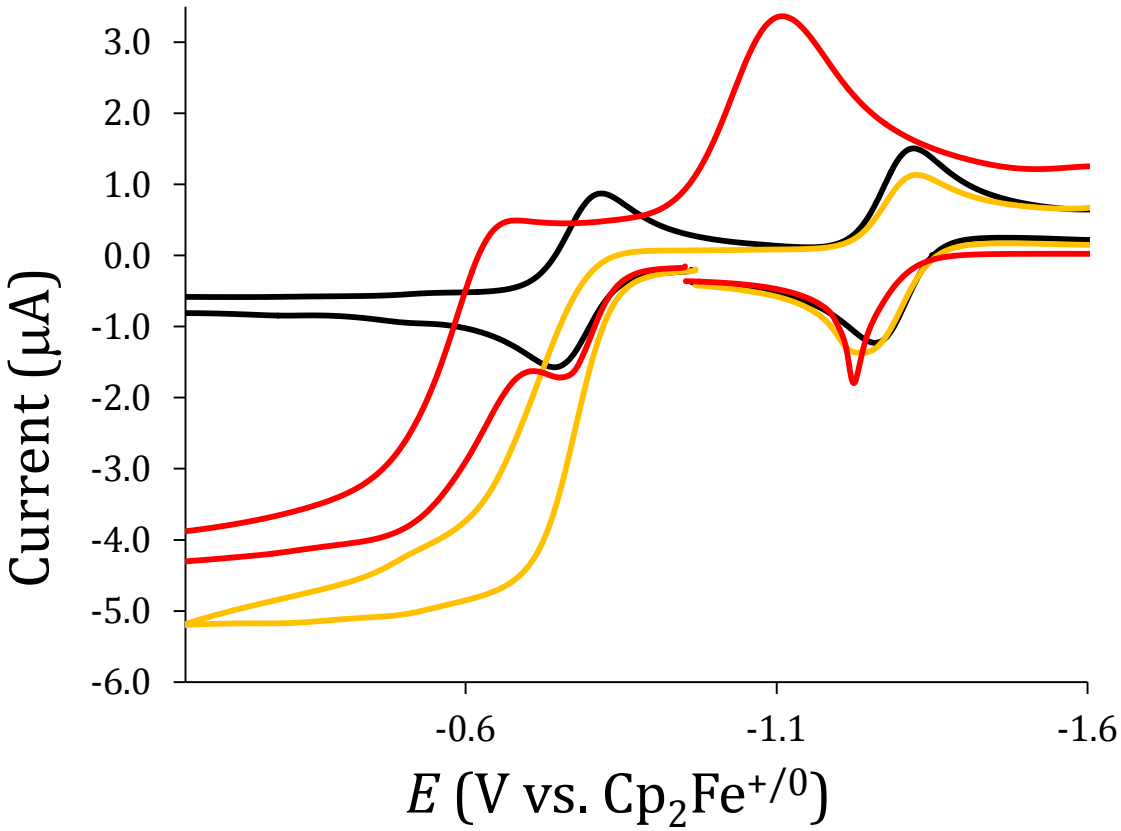

Figure S13. Electrochemistry of **[2]**$^{+}$ under N_2 (black), under H_2 with 5 M H_2O (red) or under H_2 with 0.03 M triethylamine (orange). The return wave at -1.1 V is assigned to the reduction of one of the protonated intermediates. Conditions: 0.2 M NBu_4PF_6 acetonitrile solutions, 100 mV/s, glassy-carbon working electrode. Catalyst concentration: 0.75 mM.

References

1. R. A. Heintz, J. A. Smith, P. S. Szalay, A. Weisgerber and K. R. Dunbar, *Inorganic Synthesis*, 2002, **33**, 75.
2. J. Y. Yang, S. Chen, W. G. Dougherty, W. S. Kassel, R. M. Bullock, D. L. DuBois, S. Raugei, R. Rousseau, M. Dupuis and M. Rakowski DuBois, *Chem. Commun.*, 2010, 8618-8620.
3. S. Lense, M.-H. Ho, S. Chen, A. Jain, S. Raugei, J. C. Linehan, J. A. S. Roberts, A. M. Appel and W. Shaw, *Organometallics*, 2012, **31**, 6719-6731.
4. B. R. Galan, J. Schoffel, J. C. Linehan, C. Seu, A. M. Appel, J. A. S. Roberts, M. L. Helm, U. J. Kilgore, J. Y. Yang, D. L. DuBois and C. P. Kubiak, *J. Am. Chem. Soc.*, 2011, **133**, 12767-12779.
5. M. Rakowski DuBois and D. L. DuBois, *Chem. Soc. Rev.*, 2009, **38**, 62-72.
6. A. M. Appel, D. H. Pool, M. O'Hagan, W. J. Shaw, J. Y. Yang, M. Rakowski DuBois, D. L. DuBois and R. M. Bullock, *ACS Catalysis*, 2011, **1**, 777-785.
7. K. Fraze, A. D. Wilson, A. M. Appel, M. Rakowski DuBois and D. L. DuBois, *Organometallics*, 2007, **26**, 3918-3924.
8. R. Kelly, J. Page, Q. Luo, R. Moore, D. Orton, K. Tang and R. Smith, *Anal. Chem.*, 2006, **78**, 7796-7801.
9. J. Y. Yang, S. E. Smith, T. Liu, W. G. Doughtery and W. A. Hoffert, *J. Am. Chem. Soc.*, 2013, **135**, 9700-9712.
10. S. Raugei, Shentan Chen, Ming-Hsun Ho, Bojana Ginovska-Pangovska, Roger J. Rousseau, Michel Dupuis, Daniel L. DuBois and R. M. Bullock, *Chemistry - A European Journal*, 2012, **18**, 6493-6506.
11. M. O'Hagan, M.-H. Ho, J. Y. Yang, A. M. Appel, M. Rakowski DuBois, S. Raugei, W. J. Shaw, D. L. DuBois and R. M. Bullock, *J. Am. Chem. Soc.*, 2012, **134**, 19409-19424.
12. G. M. Sheldrick, Bruker AXS Inc., Madison, WI, 2004.
13. *SAINTPlus: Data Reduction and Correction Program*, Bruker AXS Inc., Madison, WI, 2004.
14. G. M. Sheldrick, University of Gottingen, Germany, 2003.
15. G. M. Sheldrick, University of Gottingen, Germany, 2007.
16. J. A. S. Roberts and R. M. Bullock, *Inorg. Chem.*, 2013.
17. E. S. Wiedner, J. Y. Yang, S. Chen, S. Raugei, W. G. Dougherty, W. S. Kassel, M. L. Helm, R. M. Bullock, M. Rakowski DuBois and D. L. DuBois, *Organometallics*, 2012, **31**, 144-156.
18. X. Duan and S. Scheiner, *J. Am. Chem. Soc.*, 1992, **114**, 5849-5856.